Experimental and Modelization Approach in the Study of Acid-Site Energy Distribution by Base Desorption. Part I: Modified Silica Surfaces

Paolo Carniti,* Antonella Gervasini,* and Simona Bennici

Dipartimento di Chimica Fisica ed Elettrochimica, Università degli Studi di Milano, via Camillo Golgi n. 19, I-20133 Milano, Italy

Received: May 17, 2004; In Final Form: October 22, 2004

The acid properties of pure and modified silica surfaces were studied by 2-phenylethylamine (PEA) desorption in a thermogravimetric (TGA) apparatus, carrying out the experiments at different heating rates ($5 < \beta/(°C \cdot min^{-1}) < 30$). The samples, containing about 13 wt % alumina, titania, and zirconia, were prepared by the sol−gel route from molecular precursors. The textural, structural, and surface properties of the materials were studied by complementary techniques (ICP, XRD, N_2 physisorption, SEM-EDS, and XPS). The chemical modification of the silica surface by enrichment with Al, Ti, or Zr, in amounts of about 90, 50, and 60% of that introduced in the preparation as determined by XPS, justified the increase of acidity of the modified silica surfaces compared with that of pure silica. The total number of strong acid sites was found to be in the order of SZ > SA > ST ≫ S. Two different kinetic approaches were applied to the thermogravimetric data to kinetically interpret the PEA desorption from the different types of acid sites. The classical differential Kissinger model was found to be inadequate in representing the very complex situation of the acid surfaces. A more complex model is proposed by simultaneously taking into account PEA desorption from the different acid sites by a set of parallel and independent desorption reactions following Arrhenius's kinetic law. The fraction of each type of acid site on each surface and the relevant activation parameters were optimized through a computational procedure. Very good fitting of the experimental−calculated desorption profiles corroborated the validity of the model. For each surface, the acid-site energy distribution is presented and discussed in relationship to the surface composition of the oxides.

Introduction

The surfaces of oxide materials are variably covered by hydroxyl groups beside highly unsaturated positive or negative ions of variable acid/base strength according to the accepted concept of acido-basicity of solids. The use of suitable probe molecules (ammonia, pyridine, methylethylamine, *tert*-butylamine, etc.) permits the quantitative analysis of the solid's acidity by adsorption from zero coverage to partial or full surface coverage of the acid sites or by desorption from completely saturated acid sites with the probe. The spectroscopic techniques of FT-IR,[1] XPS,[2,3] and MAS NMR,[4] among others, are employed to elucidate the nature of the molecular complex formed by the basic probe adsorption on the acid site. The thermal physicochemical techniques of calorimetry,[5−7] thermogravimetry,[8,9] and temperature-programmed desorption analysis,[10−15] among others, are more suitable in determining the thermal effects of the acid/base adsorption reaction related to the strength and strength distribution of the acid sites without selectively individuating their different nature.

Thermal desorption techniques (TPD) have gained great popularity because of the ease of operative actualization and the possibility of probing the bonding between a particle and a solid surface. Although there is widespread use of TPD in studies of the surface acidity of solid catalysts by using suitable base probes (ammonia and pyridine, among others), it is worth noting that the desorption profiles are often poorly resolved and curve-deconvolution methods are needed to gain insight into kinetic interpretation. Various mathematical analyses of the thermodesorption profiles have been proposed by different authors to provide information about the distribution of acid strength, either taking readsorption effects into account or not.[10,11,16−20] A different and simpler approach that can be pursued in the determination of kinetic parameters is based on the analysis of thermodesorption curves collected at different heating rates (β). The shift of the temperature of the maximum rate of desorption (T_{max}) as a function of β can be considered to obtain the activation energy (E_a) of the desorption reaction by means of different model equations. Such an approach was applied to different kinds of reactions (e.g., degradation of polymers, desorption from surfaces, etc).[21−24] In the case of desorption of molecules from heterogeneous surfaces with different kinds of sites, different peaks of desorption can be detected with different T_{max} values. For each peak, the shift of T_{max} has to be considered to derive the activation energy distribution. For the application of this approach, the thermodesorption curves have to be well defined with clearly detectable T_{max} values. When convoluted and poorly resolved curves are obtained, this method does not provide reliable kinetic results. Moreover, the usual model equations have the viewing of the whole desorption process as a series of successive desorption reactions as a common point. In the case of base desorption from acid surfaces, for example, the lower the temperature of desorption, the weaker the acid site. This can be a restrictive viewing when very heterogeneous and complex surfaces are concerned. Simultaneous desorption reactions could occur during

* To whom correspondence should be addressed. E-mail: paolo.carniti@unimi.it; antonella.gervasini@unimi.it. Tel: 0039-02-50314-261/254. Fax: 0039-02-50314300.

10.1021/jp047889g CCC: $30.25
Published on Web 01/06/2005

the desorption process from surface sites or with different electronic or geometric structure. An improved model that takes into account the possibility of simultaneous desorption from the different surface sites is expected to deepen the kinetic interpretation of complex surfaces, starting from experimental thermodesorption curves collected at different β values. An analogous approach was applied in studying the heterogeneity of oxidic and catalytic surfaces by the adsorption of ammonia or nitrogen monoxide probes. The simultaneous adsorption on all of the different kinds of sites was assumed for the evaluation of the different enthalpies of adsorption.[25−28]

Silica powders are widely used in industry as fillers, catalysts, catalyst supports, adsorbents, and chromatographic agents, among other applications. Silica is a covalent oxide, and it can be considered to be a neutral surface in the sense that there is a balanced charge distribution among the various atoms forming the surface. On the silica surface, Lewis acidity is completely absent, and only surface hydroxyl groups are formed, which are responsible for weak Brönsted acidity. There is the possibility of modifing the acid properties of the silica surface by chemical modification, for example, by covalent anchoring of acid groups,[29] or by introducing lower-valence elements, which create a defect of charge, causing the formation of a strong Brönsted site to balance it.[30] This is the well-known case of silica−alumina in which the introduction of Al in amorphous silica gives rise to a strong acid solid widely used in oil refining and the chemical industry, besides being a support for active catalytic phases.[31]

The aim of the present study was to characterize the acidity of modified silica surfaces that have been synthesized by the classical sol−gel route, which ensured the material preparation under the control of texture and composition. The amount of guest element (Al, Ti, or Zr) introduced in the host silica structure was similar to the amount of Al present in the silico-alumina used as a support for de-NO_x catalysts; these results have been recently reported.[31] The material's acid properties were determined by studying the thermal desorption of a base probe molecule carried out in a thermogravimetric analyzer. Thermal analysis techniques are widely used for both gas-adsorption and gas-desorption experiments to determine thermodynamic (e.g., adsorption enthalpy) or kinetic (e.g., activation energy) parameters of the surface sites of solids.[32,33] Many methods were developed to interpret thermoanalytical data kinetically under nonisothermal conditions; they have been reexamined in an attempt to increase the reliability of the kinetic parameters obtained[24,32] and, recently, to propose original work methodologies.[33−35]

Concerning the base probe molecule use, we employed 2-phenylethylamine (PEA), which has been successfully used to determine, with a pulse liquid chromatographic technique,[36] the acidity of catalysts employed in the catalytic hydrolysis and dehydration of polysaccharides and sugars in aqueous solvents.

The thermodesorption curves have been interpreted kinetically by both a conventional and a novel kinetic model. The proposed model was applied to the curves obtained at the different heating rates ($5 < \beta/(°C \cdot min^{-1}) < 30$) and was able to fit the experimental desorption profiles satisfactorily, therefore obtaining the kinetic and activation parameters for each type of acid site. This allowed us to map the acid sites of the surfaces from an energetic point of view.

Experimental Section

Sample Preparation. Pure-grade reagents from Fluka and Merck-Schuchardt were utilized for the synthesis of the oxide materials. Pure silica (S) and modified silicas with Al (SA), Ti (ST), and Zr (SZ) were synthesized via the sol−gel route. Tetraethyl orthosilane, $Si(OC_2H_5)_4$ (TEOS), aluminum triisopropylate, $Al[(CH_3)_2CHO]_3$, tetraethyl orthotitanate, $Ti(OC_2H_5)_4$, and zirconium propoxide, $Zr(OC_3H_7)_4$ (solution 70% in propanol) were the sources of Si, Al, Ti, and Zr, respectively. Base-catalyzed hydrolysis of TEOS, adapting the method described by Perego et al.,[37] was performed for the SA and ST syntheses. SZ was synthesized following the procedure reported by Serrano et al.,[38] including acid-catalyzed hydrolysis of TEOS. Ethyl alcohol (99.8% v/v), water, and tetrapropylammonium hydroxide solution (20% in water, TPA−OH) as the gelling agent were used for the synthesis of SA or ST; 1-propanol, hydrochloric acid as the catalyst, and ammonia as the gelling agent were used for the synthesis of SZ. The molar ratios in the reagent mixtures were 0.15, 0.10, and 0.08 for Al/Si, Ti/Si, and Zr/Si, respectively. The obtained gel was aged for 18 h at room temperature,dried at 120 °C for 6 h, and calcined at 550 °C for 8 h.

Characterization Techniques and Procedures. The Al, Ti, and Zr content of the powders was measured by ICP (inductively coupled plasma, from Spectro) after dissolving the sample in aqua regia and HF; then a solution of HCl was made.

The nitrogen adsorption/desorption isotherms were obtained at liquid-nitrogen temperature (−196 °C) by using a Sorptomatic 1900 version instrument from Thermo-Finnigan. Prior to the analysis, weighed portions of the calcined samples (0.05 g) were outgassed for 16 h at 350 °C under a residual pressure of 10^{-3} Torr. Moreover, all of the prepared powders were examined after thermal treatment in the 120−900 °C temperature range at different times (from 8 up to 60 h) using a Micromeritics Gemini automatic apparatus for surface area determination. In this case, the samples were purged for 2 h in flowing nitrogen at the relevant temperature of thermal treatment.

Scanning electron micrographs (SEM) were obtained with a JEOL JSM-5500LV instrument. The samples were analyzed under moderate vacuum (0.15 Torr) without gold coating. Semiquantitative EDS analysis was performed with X-ray energy of 20 kV.

XRD diffraction analyses of the powder samples were collected with a Philips PW1710 vertical goniometric diffractometer using a Ni-filtered Cu Kα1 radiation ($\lambda = 1.54178$ Å). The chamber rotated around the sample at $1° \ 2\theta \cdot min^{-1}$; the range of investigation was from 5 to 75° 2θ.

X-ray photoelectron spectra (XPS) were collected in an M-Probe apparatus (Surface Science Instruments). The X-ray source provided monochromatic Al Kα radiation (1486.60 eV). The residual pressure in the analysis chamber was typically 5×10^{-9} Torr. Charge effects were compensated for by the use of a flood gun (3 eV). A spot size of 400×1000 μm^2 and a pass energy of 150 eV were used for the collection of survey spectra. The calibration of the spectra was performed with the Si 2p line from silica−alumina (103.3 eV). This reference, in agreement with the literature data, was consistent with the C 1s peak of adventitious carbon at a binding energy (BE) of 284.8 eV. The other BE values were measured at 154 (Si 2s), 75 (Al 2p), 459 (Ti $2p_{3/2}$), and 185 (Zr 3d) with an accuracy of ± 0.20 eV.

Acidity Determination. The thermogravimetric analyses (TGA) of 2-phenylethylamine (PEA) desorption from the saturated powders were performed by a TGA 7 Perkin-Elmer thermal analyzer. The calibration of temperature was performed by measuring the Curie transitions (T_C) of high-purity reference materials (alumel, nickel, perkalloy, and iron; T_C of 163, 354,

SCHEME 1: Comparison between the Kissinger and the Proposed Kinetic Models for the Description of Thermal Desorption of PEA from Different Surface Acid Sites (S_i)

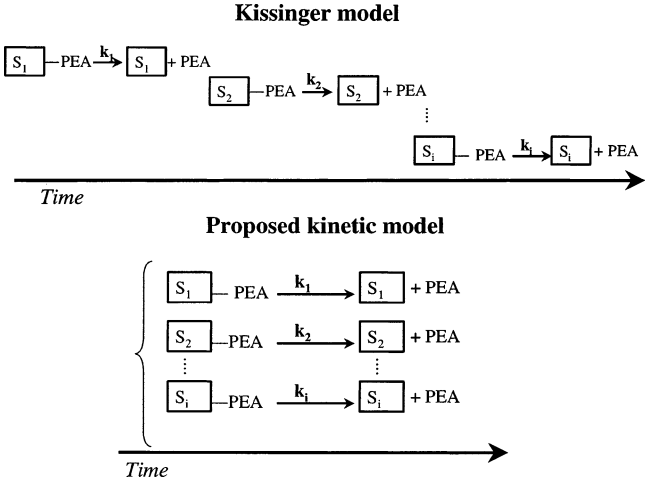

596, and 780 °C, respectively) at each different heating rate (β) employed. Prior to the TGA analysis, the powder was outgassed for 16 h at 350 °C under a residual pressure of 10^{-3} Torr. The powder was transferred in a glass cell equipped with connections for a vacuum/gas line, and liquid PEA (purity >99% from Fluka) was introduced into the cell to cover the powder completely. The slurry rested at room temperature under N_2 flow for 3 h. Then, the excess nonadsorbed PEA was removed by filtration; the operation was carried out under N_2. The obtained saturated powder was loaded on the pan of the TGA (10−15 mg), and a two-step analysis was carried out, both under N_2 flowing at 30 mL·min^{-1}. The first isothermal step was carried out at 50 °C to remove all of the excess PEA from the surface, and it lasted until a constant mass was reached. The second step was carried out at constant heating rates (β) of 5, 10, 15, 20, and 30 °C·min^{-1} from 50 up to 800 °C to remove PEA from the surface completely. The total mass loss of PEA (g_{PEA}) was determined by subtracting the final mass at 800 °C from the mass obtained at the end of the isothermal step. Intermediate PEA mass losses ($g_{PEA1,2,..n}$) were determined by employing the differences between the final mass at 800 °C and the masses observed at a definite time of analysis corresponding to the well-defined steps of the thermogram. Assuming 1:1 stoichiometry for the PEA adsorption on the acid site, the total number of sites on the surface could be known and expressed as the equivalent of acid sites per unit mass of oxide (equiv/g_{oxide}). Intermediate PEA mass losses corresponded to the number of acid sites of definite acid strength. The derivative of the TGA curves (DTGA) gave the temperatures at which the maximum rate of PEA desorption occurred (T_{max}) from the acid sites of definite strength.

The classical differential Kissinger equation[39] was used to obtain indicative values for the activation energy of the PEA desorption, exploiting the observed shift of the T_{max} values with the heating rates (β) (Scheme 1).

Modeling and Computation. The model that was developed took into account the possibility of a simultaneous desorption of the probe amine from the different kinds of surface acid sites as represented in Scheme 1. The PEA desorption was regarded as a set of different simultaneous independent first-order reactions, each one relevant to a single type of site. The desorption reactions were considered to follow Arrhenius' law. All of the surface sites that were able to retain the amine chemically were supposed to be saturated at the beginning of the thermal programmed desorption. The occurrence of readsorption of the desorbed amine molecules, often considered in the interpretation of thermal desorption data,[12,16,18] was not taken into account because of the thin package of the powder and the large pore diameter of the materials. These conditions allowed a free departure of the amine once it had broken the bond with the acid site.

According to the kinetic model, the time course of PEA desorption in a thermal programmed desorption is described by the following set of equations

$$\begin{cases} dT/dt = \beta \\ -dx_1/dt = [A_1 \exp(-E_{a,1}/RT)]x_1 \\ -dx_2/dt = [A_2 \exp(-E_{a,2}/RT)]x_2 \\ \cdots\cdots\cdots\cdots \\ -dx_n/dt = [A_n \exp(-E_{a,n}/RT)]x_n \end{cases} \quad (1)$$

$$x_1^\circ + x_2^\circ + \ldots\ldots + x_n^\circ = 1 \quad (2)$$

with n being the number of different types of sites on the surface, x_i ($i = 1, 2,..., n$) being the residual fraction of PEA on the ith type of site at time t, and x_i° being the analogous fraction at zero time, corresponding to the fraction of sites of the ith type.

The parameters of the model to be determined were n, x_i°, A_i, and $E_{a,i}$ with $i = 1, 2,..., n$. At different given values of n, the other parameters were obtained by employing a computer program that utilizes the optimization subroutine OPTNOV.[40] The set of differential equations was integrated by a fourth-order Runge−Kutta numerical method.[41] The objective function to be minimized was

$$\Phi = \sum_j \sum_k (x_{calcd,j,k} - x_{exptl,j,k})^2 \quad (3)$$

where $x_{calcd,j,k}$ and $x_{exptl,j,k}$ are the calculated and the experimental PEA residual fractions on the surface, respectively, at time t_j and heating rate $\beta = \beta_k$; $x_{calcd,j,k} = (x_1 + x_2 + \ldots\ldots + x_n)_{j,k}$. All the experimental data relevant to a given solid, obtained with the different heating rates, were taken into account at the same time during the computations. The indicative values obtained by the Kissinger approach were employed as starting values for the parameters to be optimized.

Results and Discussion

Sample Preparation and Characteristics. The critical step for the material preparation was the gel formation, deriving from the addition of a Si precursor (TEOS) into a solution of an Al or a Ti precursor in TPAOH or from the addition of a Zr precursor to an acidic solution of TEOS.[37,38] Clear and well-homogenized hydrogels were observed in the case of silica synthesis, whereas the hydrogels for the syntheses in the presence of Al, Ti, and Zr were opalescent. The samples obtained by gelation showed the same Al/Si, Ti/Si, and Zr/Si molar ratios as those in the reagent mixtures. After the drying and calcination steps, the obtained powders were fully characterized for their texture, structure, and surface properties.

From ICP analysis, the weight amounts of Al_2O_3, TiO_2, and ZrO_2 could be calculated; they ranged from 12 to 14% (Table 1). The semiquantitative SEM-EDS analysis of the powders showed homogeneous Ti distribution in the surface layers (analysis depth of about 1 μm) with an amount close to but smaller than that of the bulk. Conversely, very heterogeneous Al and Zr distributions could be observed as revealed by X-ray mapping of the oxide grains. None of the Al- and Zr-containing silicas presented segregated phases as demonstrated by the

TABLE 1: Textural and Surface Properties of the Studied Oxides[a]

code	co-oxide (wt %)	S (m^2/g)[a]	V_p (cm^3/g)[a]	d_{av} (nm)[a]	M/(Si + M)[a,b]	surfacing[a,c] (%)
S		387	1.04	8.4		
SA	12.2	777	0.85	3.5	13.2	90
ST	13.2	494	0.69	4.3	5.9	51
SZ	14.3	596	1.69	1.6−7.4	5.4	62

[a] Determined on the calcined samples. [b] Determined by XPS, M = Al, Ti, or Zr. [c] Surface-to-bulk ratio: $(M/Si)_s/(M/Si)_b$.

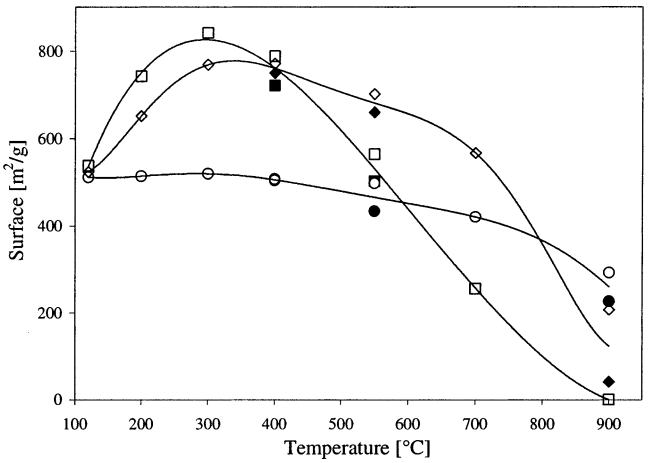

Figure 1. Trend of surface area as a function of temperature for the modified silicas: (◊) SA, (□) ST, and (○) SZ. The starting point corresponds to dried (120 °C) samples; each successive temperature was maintained for 8 h. At 400, 550, and 900 °C, the surfaces were measured after both 8 and 60 h (filled symbols).

complete amorphous character of the powders, measured after calcination at different temperatures ranging from 300 to 900 °C.

The surface areas, total pore volumes, and average pore diameters of the studied samples were presented in Table 1. It is well known that temperature can affect the textural properties of an oxide material, in particular, the surface area extension. In this perspective, the prepared powders were examined after thermal treatment in the 120−900 °C temperature range for different times. Figure 1 shows the trend in the surface area as a function of temperature for SA, ST, and SZ. The trend observed for SZ is worth noticing; its surface maintained a value of around 500 m^2/g over a large range of temperature (120−550 °C) followed by a slight decrease in surface area, which dropped to 293 and 227 m^2/g at 900 °C for 8 and 60 h, respectively. The trends observed for SA and ST were more usual; the surface area passed through a maximum in correlation with pore depletion at 300 °C for ST and around 300−400 °C for SA. For the highest temperatures, a decisive decrease in surface area was observed with values approaching zero for ST, whereas for SA maintained at 900 °C, values of 210 and 42 m^2/g for 8- and 60-h treatments, respectively, were obtained. The amorphous character of the powders was maintained in every case independent of time and temperature of treatment as confirmed by XRD analysis. Comparatively, the pure silica surface passed from 387 m^2/g (calcined at 550 °C) to about zero surface for the thermal treatment at 900 °C, with the formation of a cristobalite crystalline phase.

XPS spectroscopy confirmed the presence of Al, Ti, and Zr on the modified silica surfaces. From the experimental atomic concentrations obtained, it was possible to calculate the molar M/(Si + M) surface ratios (Table 1). The surfacing of Al, Ti, and Zr could be determined by comparing these ratios with the bulk ratios, as reported in the last column in Table 1. Because of the lesser atomic mass of Al in comparison with that of Ti and Zr, the Al surfacing was the highest among the three guest elements. The presence of the guest metals at the silica surface is a key point in guaranteeing the enhancement of the acidity of the modified silica surfaces.

Acidity Study. *Base Thermodesorption Analysis.* PEA, the amine probe used to characterize the surface acidity of the samples, has a high basicity ($pK_{a,PEA} = 9.84$; $PA_{PEA} = 936.2$ kJ/mol) comparable with that of a conventionally used basic probe, such as ammonia. PEA is a probe that has already been utilized for titrating the acidity of catalytic solids in solution (aqueous or organics) by a pulse liquid chromatographic technique utilizing a UV detector ($\lambda = 254$ nm).[36] For thermogravimetric measurements, PEA is particularly useful because of its high molecular mass ($M = 121.18$ g/mol).

The thermal desorption of PEA from the surfaces was realized while monitoring the mass loss during the two-step analysis detailed above. The first isothermal step (50 °C) was aimed at desorbing the excess PEA multilayering deposited on the surface. In every case, after sufficient time, a constant value of mass was gained with a well-defined plateau versus time analysis. The mass obtained at the plateau was considered to be the initial mass of the sample being studied, covered by a monolayer of PEA. The second-step analysis was carried out by increasing the temperature at a constant rate from 5 up to 30 °C·min^{-1} (from 50 up to 800 °C), and it was intended to desorb PEA completely from the acid sites of the surface. The final mass obtained at 800 °C corresponded to the catalyst mass to which the number of acid sites determined ($equiv_{site}/g_{oxide}$) refers. In any case, any carbon residues could not be observed on the powders after the two-step analysis, thus proving the total removal of PEA from the surfaces.

Because temperature affects the extent of the surface area of the oxides to a lesser or higher extent, the high temperatures used during the thermal desorption of PEA could cause sintering of the surfaces, partly invalidating the observed phenomenon of PEA desorption from the acid sites. To take this important point into account, we estimated the values of the rate and activation parameters of the process leading to the surface area decrease in the temperature range of 550−800 °C, starting from the experimental data of Figure 1. The samples stayed in the 550−800 °C temperature range for 50 and 8.3 min for heating rates of 5 and 30 °C/min, respectively. Unimportant decreasing of the surface area for SA could be calculated in the 550−800 °C range for the times of stay at these high temperatures (1.1 and 0.2% for heating rates of 5 and 30 °C/min, respectively) and a very limited one for SZ (0.5 and 0.1% for heating rates of 5 and 30 °C/min, respectively). ST is the sample that underwent to the highest decrease of surface area (5.4 and 0.9% for heating rates of 5 and 30 °C/min, respectively). In light of this data, we decided to interpret the thermodesorption curves numerically up to 600 °C.

Figure 2 comparatively reports the thermograms for PEA desorption from the four samples obtained for $\beta = 10$ °C/min, reconstructed by plotting the amount of PEA desorbed per unit mass of oxide (g_{PEA}/g_{oxide}). The isothermal step at 50 °C lasted 600 min; within this time frame, well-defined plateaus were obtained, in any case. From the plateau height, the total amount of PEA desorbed could be obtained (Table 2, second column). Such an amount roughly corresponded to the amount of PEA able to cover the surface close to but lower than the monolayer (4−5 $\mu equiv/m^2$). The second nonisothermal step of analysis showed decreasing curves down to zero. The desorption curves

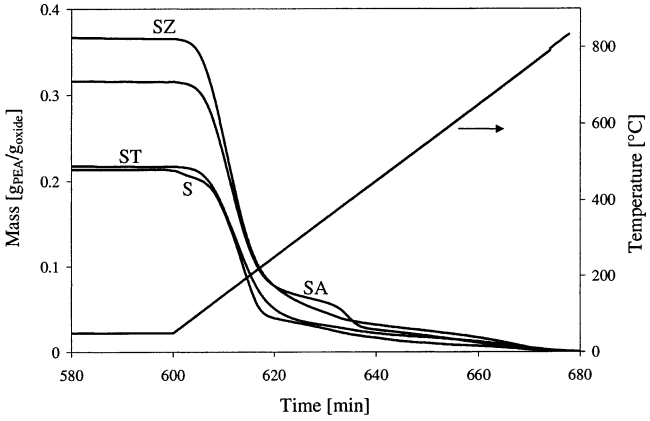

Figure 2. Thermogravimetric curves of PEA desorption from saturated samples. First-step analysis corresponds to the isothermal analysis at 50 °C, and second-step analysis corresponds to the heating rate (10 °C/min) up to 800 °C.

TABLE 2: Number and Distribution of Acid Sites Evaluated by Experimental PEA Thermodesorption

	total sites			
code	$[\text{mequiv/g}]_{tot}$	$[\mu\text{equiv/m}^2]_{tot}$	$F_{T_{max,1}}{}^a$	$F_{T_{max,2}}{}^b$
S	1.87	4.84	0.90	0.10
SA	2.75	3.54	0.82	0.18
ST	1.79	3.62	0.90	0.10
SZ	2.94	4.94	0.90	0.10

[a] Fraction of acid sites determined from PEA mass loss relevant to the $T_{max,1}$ peak. Average value from TGA experiments performed at different β values. [b] Fraction of acid sites determined from PEA mass loss relevant to the $T_{max,2}$ peak. Average value from TGA experiments performed at different β values.

have different shapes reflecting the different acid-site distribution on the surfaces. The first derivative of the TGA curves (DTGA) showed the inflection points as negative peaks; the minimum of each peak represented the time and temperature at which the rate of PEA desorption was maximized (t_{max}/T_{max}). When more than one DTGA peak is observed, it can be assumed that sites of different acid strength are present on the surface.

Two distinct types of acid sites, associated with $T_{max,1}$ and $T_{max,2}$ temperatures, were observed on the surfaces of SA, ST, and SZ, but only one was observed on that of S. The $T_{max,1}$ values associated with the first type of site are near the boiling temperature of PEA (T_b = 198−200 °C at atmospheric pressure), in any case. It can be assumed, then, that the PEA fraction desorbing at $T_{max,1}$ ($F_{Tmax,1}$), which corresponded to 80−90% of the total amine desorbed (Table 2), was weakly bound to the surface sites. However, the much higher $T_{max,2}$ values observed reflected acid sites able to adsorb the basic molecule strongly. The fraction of sites associated with $T_{max,2}$ is very small for the S, ST, and SZ samples, whereas SA shows a higher fraction of strong acid sites. The number of sites associated with $T_{max,2}$ is 0.495, 0.294, 0.187, and 0.179 mequiv/g for SA, SZ, S, and ST, respectively. A different order could be found when the number of acid sites was viewed per unit surface because of the wide difference in surface area among the samples (Table 2).

A number of methods for the calculation of kinetic parameters from thermodesorption curves have been developed. Some methods allow the calculation of all of the kinetic parameters, whereas with others, only some parameters can be obtained. Some methods require an assumption of the reaction order, and the correctness of the results for other kinetic parameters depends on the accuracy of this assumption. They can involve either a single thermogram or multiple thermograms with different constant heating rates. For example, the differential Freeman and Carroll method allows the calculation of the activation energy from a single thermogram obtained at a constant heating rate. With the basic assumption of a first-order reaction, the activation energy is determined by drawing a linear plot; nonlinearity in this plot indicates a change in mechanism. Among the methods based on multiple heating rate experiments, the integral methods of Ozawa and Kissinger are the most popular. They differ only in the method adopted to integrate the rate expression containing the temperature-dependent function and composition-conversion-dependent term.[24] The expression given by Kissinger has been used in this work.

The Kissinger equation makes the determination of the activation energy for a decomposition reaction possible, according to the original derivation,[39] regardless of reaction order

$$\frac{\beta E_a}{RT_{max}{}^2} = A\alpha(1-x)_{max}{}^{(\alpha-1)} \exp\left(\frac{-E_a}{RT_{max}}\right) \qquad (4)$$

with R being the gas constant, A being the preexponential factor of the Arrhenius equation, α being the reaction order (in the present case, the order of the desorption reaction), and x being the fraction reacted (in the present case, the fraction desorbed). Equation 4 can be linearized by writing it in logarithmic form. Kissinger demonstrated that the equation can also be linearized with reaction orders different from 1. Thus, by reporting ln $\beta/T_{max}{}^2$ versus $1/T_{max}$, E_a values can be obtained from the slope of the linear-regression straight lines. The T_{max} values observed for different β values, together with the calculated activation energy values (E_a) for PEA desorption for each type of site, have been collected in Table 3. Only for S, the $E_{a,1}$ value was similar to the enthalpy of vaporization (ΔH_v = 42 kJ/mol, calculated according to Trouton's rule). Higher values, from 50 to 58 kJ/mol, were obtained in the order SA < SZ < ST. For these three samples, PEA desorption at $T_{max,2}$ was associated with high values of the activation energy ($E_{a,2}$) ranging from 68 to 108 kJ/mol.

However, the obtained acid-site distribution (amount vs E_a value of each acid site) can be regarded only as indicative because of the lack of precision of the determination. In fact, for most cases, convoluted DTGA peaks that hindered the presence of other sites could be observed. Moreover, for convoluted and broadened peaks, it was not possible to determine the shifts of the T_{max} values accurately for different heating rates (β).

Modeling of Thermodesorption Curves. The kinetic model described in the Experimental Section was applied to the experimental data of PEA thermodesorption to obtain more reliable kinetic parameters for PEA desorption than those obtained by the conventional Kissinger method as well as a more accurate evaluation of the distribution of the different types of acid sites on the oxide surfaces.

For each oxide, the data obtained at the different β values were taken into account at the same time. Only the temperature interval from 50 to 600 °C was utilized in the computations because of the loss of surface area occurring at higher temperatures, even though it was limited as was discussed above. The values obtained by the Kissinger approach were employed as initial values of the parameters to be optimized. In the first computations, the number of different site types (n) deriving from the direct inspection of the experimental desorption profiles was utilized (n = 2 or 3). Afterward, n was increased until no significant improvement of the objective function was observed.

TABLE 3: Temperatures and Energies of PEA Desorption Evaluated by TGA Analysis and Kissinger's Model

code	β (°C/min)	$T_{max,1}$ (°C)	$T_{max,2}$ (°C)	ln A_1[a]	$E_{a,1}$ (kJ/mol)[a]	r_1[b]	ln A_2[a]	$E_{a,2}$ (kJ/mol)[a]	r_2[b]
S	10	180		12.2	36	0.992			
	15	192							
	20	208							
	30	225							
SA	5		392	12.1	50	0.944	25.7	108	0.967
	10	170	398						
	15	193	403						
	20	203	417						
	30	209	429						
ST	5	168	382	19.5	58	0.990	16.9	68	0.962
	10	182	398						
	15	194	432						
	20	207	451						
	30	213	460						
SZ	5		360	14.3	57	0.994	10.3	97	0.982
	10	167							
	15	176	387						
	20	183							
	30	195	420						

[a] Determined by the Kissinger equation; A (min^{-1}). [b] Linear correlation coefficient.

TABLE 4: Optimized Parameters Obtained from the Kinetic Model

code	site type	site fraction	site (μequiv/m^2)	ln A (A/min^{-1})[a]	E_a (kJ/mol)	k_{300} (min^{-1})[b]	σ[c]
S	1	0.43	2.06	10.9	45	4.73	0.018
	2	0.47	2.30	14.3	65	2.09	
	3	0.05	0.25	11.3	69	0.04	
	4	0.05	0.22	10.8	96	9×10^{-5}	
SA	1	0.66	2.34	11.5	48	4.02	0.014
	2	0.14	0.48	16.5	100	0.01	
	3	0.14	0.50	26.1	118	4.07	
	4	0.06	0.21	14.1	121	1×10^{-5}	
ST	1	0.51	1.85	13.7	55	9.20	0.016
	2	0.34	1.23	16.0	72	2.22	
	3	0.10	0.35	15.9	91	0.04	
	4	0.05	0.18	37.2	283	2×10^{-10}	
SZ	1	0.60	2.98	12.7	50	8.55	0.013
	2	0.21	1.05	16.7	75	3.03	
	3	0.11	0.53	13.2	77	0.05	
	4	0.08	0.38	23.7	183	4×10^{-7}	

[a] A [min^{-1}]. [b] Rate coefficients of PEA desorption calculated at 300 °C. [c] Standard error of the estimates (PEA desorbed fractions).

At any given n, the parameters optimized were x_i°, ln A_i, and $E_{a,i}$ with $i = 1, 2, ..., n$. In general, a unique value of ln A_i was initially optimized for all of the sites of the same sample, allowing the program to find the best x_i and $E_{a,i}$ values. Starting from this point, all of the parameters were reoptimized in the final computations. Because the maximum value of n employed was 4, the maximum number of parameters to be optimized at the same time was 11. The very high number of experimental points (from 670 to 1155 distributed on 4 or 5 different heating rates (β) for each sample) guaranteed the possibility of attaining sound parameters.

The final results of the computations are shown in Table 4. The comparisons between the experimental and the calculated thermograms are shown in Figure 3. The satisfactory quality of the fit can be evaluated on the basis of the standard error of the estimates (σ, reported in Table 4) of the total residual fraction of PEA on the surface as well as of the representation of the calculated versus the experimental fraction of PEA desorbed, as reported in Figure 4 with SA and SZ as examples. The deviations of the calculated desorbed fractions were well inside a ±10% deviation, except for extremely low values, and any trend with β could not be observed.

The global thermogravimetric curves were also decomposed into calculated curves relevant to the various types of acid sites, as shown in Figure 5 with SA and SZ as examples. The decomposition enlightens the occurrence of both successive and simultaneous desorptions of the amine molecule from the different sites in agreement with the proposed kinetic model (Scheme 1). In particular, PEA adsorbed on site 3 of SA starts desorbing before the complete desorption from site 1, whereas sites 2 and 4 release PEA in successive steps. For SZ, PEA desorption from site 2 starts before the complete uncovering of site 1. An analogous consideration can be made by comparing sites 2 and 3. Such a kinetic aspect of the desorption mechanism is not considered by most conventional models (e.g., Kissinger equation), which are not able to interpret the desorption process from complex surfaces adequately.

An inspection of Table 4 indicates that site 1 fractions have activation energies of PEA desorption between 45 and 55 kJ/mol for all of the samples with the same order of $E_{a,1}$ values obtained by the Kissinger approach. However, the fraction attributable to such weak acid sites is much lower than that directly obtained from the thermograms (Table 2).

For all of the samples, three different types of stronger acid sites could be recognized. Considering site fractions higher than 10%, only one strong site type was found for S, and two types were found for SA, ST, and SZ. The activation energy for such sites ranged from 65 to 118 kJ/mol. Very low fractions of sites

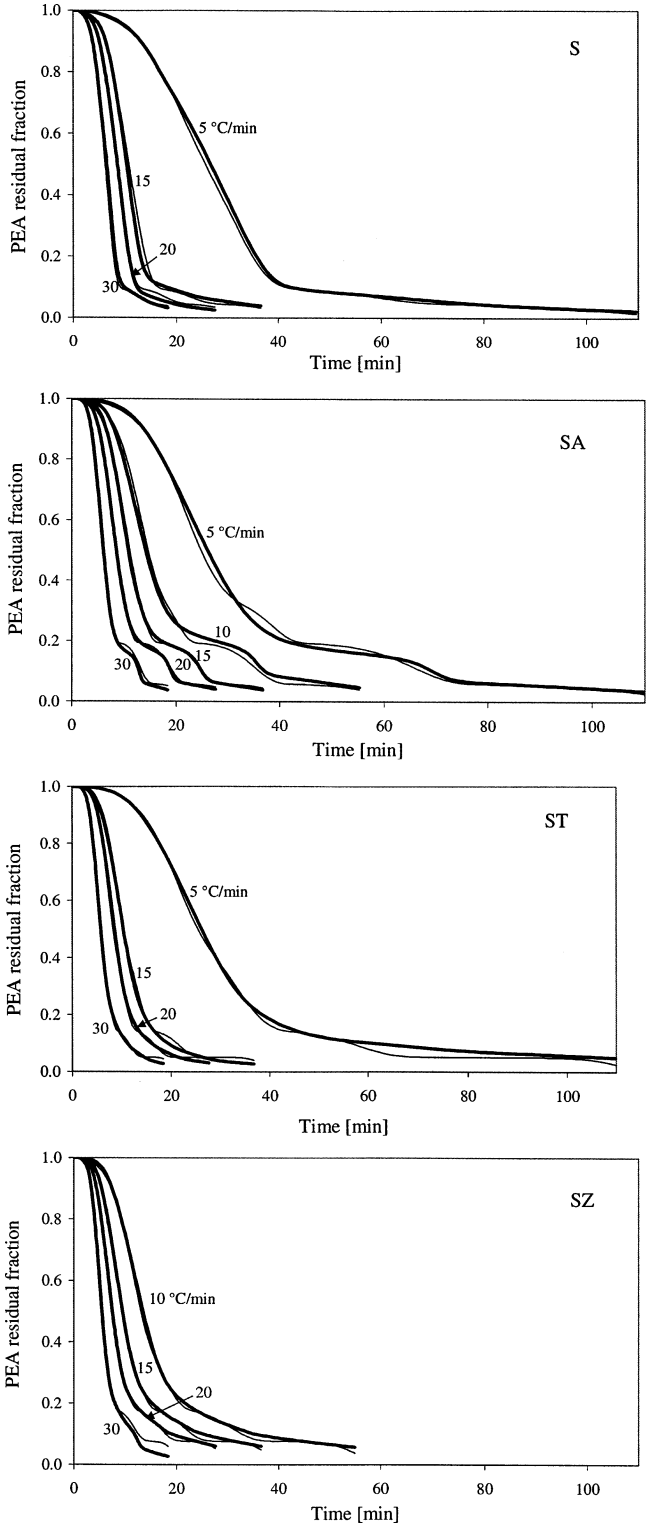

Figure 3. Thermogravimetric curves of PEA desorption (second-step analysis) from 50 to 600 °C at various heating rates (β, in °C/min) as a function of time for S, SA, ST, and SZ. Bold lines, experimental; light lines, calculated curves. The curves were calculated with the optimum parameters of Table 4.

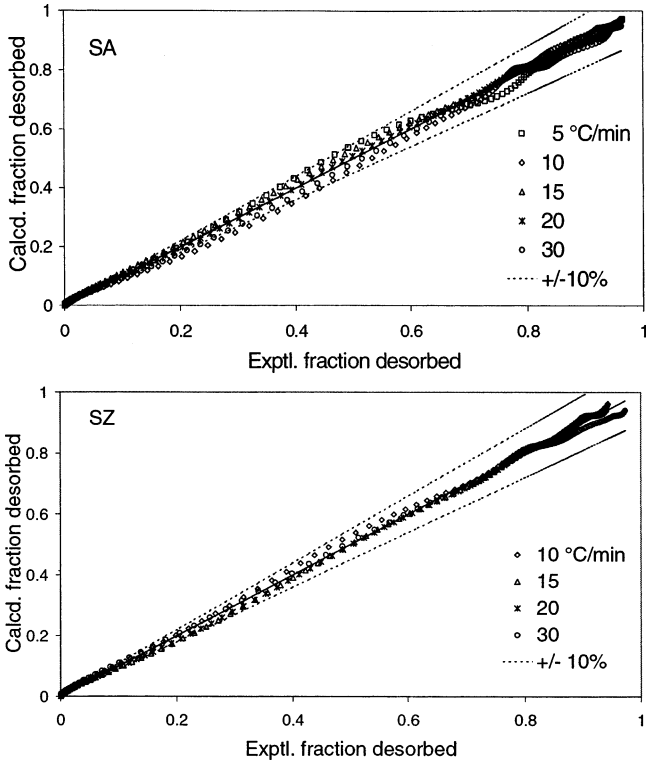

Figure 4. Calculated fractions of PEA desorbed, reported against the experimental fractions at various heating rates (β, in °C/min) for SA and SZ. Dotted lines represent the ±10% error envelope.

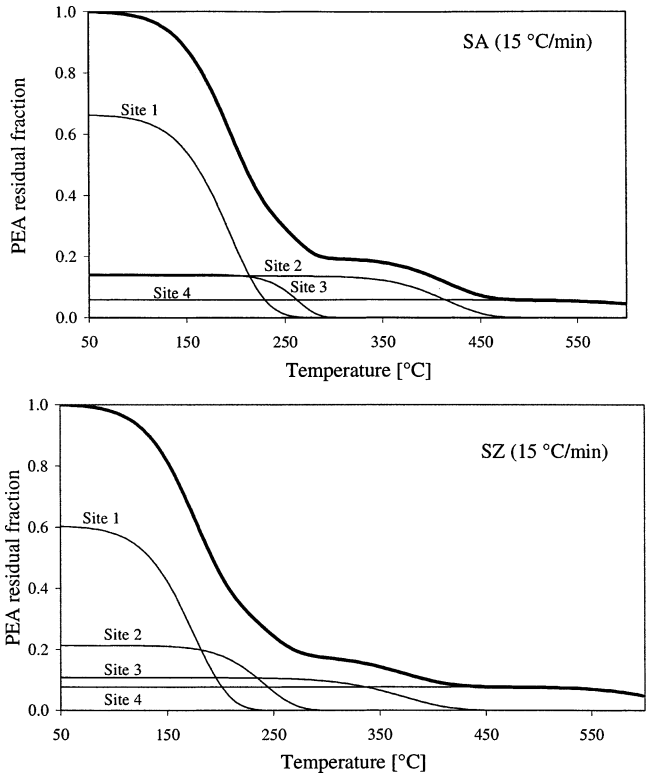

Figure 5. Decomposition of the experimental thermogravimetric curve of PEA desorption. Bold lines, overall; light lines, calculated desorption curves for each type of acid site (Table 4) for SA and SZ (β = 15 °C/min).

(≤10%) with high activation energies were also observed. The highest E_a values (183 and 283 kJ/mol for SZ and ST, respectively) could be overestimated because of the well-known compensation effect between E_a and the corresponding preexponential factor (A) often observed in heterogeneous catalysis.[42−44] Because of this effect, an increase of the activation energy relevant to the type of site ($E_{a,i}$), during the optimization procedure could go on with a parallel increase of the preexponential factor (A_i) with little or no change of the objective function. This fact should be more remarkable when few fractions of sites are concerned. It is not easy to find experi-

mentally determined preexponential factors for desorption with which to compare the present values. Desorption preexponents have been calculated in the $10^{13}-10^{19}$ s^{-1} range, as recently reported by Gellman et al.[45] in studying the desorption of straight-chain alkanes from graphite surfaces. High values can be expected when translational freedom in the transition state to desorption is greater than that in the adsorbed state. Therefore, the greater the values of the preexponential factor are, the higher the immobilization of the probe in the adsorbed state could be. In the present case, the ln A values lie within a wide interval (10−26) that corresponds to A values in the 10^4-10^{14} s^{-1} range. Preexponentials within the same range (10^4-10^8 s^{-1}) were reported for ammonia desorption from zeolite substrates.[10,16]

The order of the acidity of the sites for the different samples can be viewed as usual in terms of the number of sites per unit mass or unit surface (Table 4) as a function of energy (desorption activation energy). SZ emerges as the surface with the highest number of very strong acid sites (0.38 μequiv/m^2 with E_a around 183 kJ/mol), and SA emerges as the surface possessing the highest fraction of sites with strong acid strength (1.19 μequiv/m^2 with E_a in the range of 100−121 kJ/mol). When the fraction of acid sites with $E_a > 70$ kJ/mol is concerned (ruling out only the weak acid sites), amounts of 1.19, 1.76, and 1.96 μequiv/m^2 for SA, ST, and SZ, respectively, can be observed (Table 4). The values are roughly similar to the number of surface species containing Al, Ti, or Zr of the modified silicas, as calculated by XPS analysis: 1.4, 1.7, and 1.2 μequiv/m^2 for SA, ST, and SZ, respectively. In the first approach, a relation between the strong acid sites and the surface species containing the guest elements seems to be evident.

The acid distribution of the sites that we have made in terms of E_a could also be determined on the basis of rate coefficients of desorption evaluated at a given temperature (k_T). In this way, the influence of both of the parameters ln A and E_a is taken into account. The k values calculated at 300 °C have been reported in Table 4. In most cases, the order in terms of rate coefficient corresponds to the relevant E_a order. The different orders obtained for SA could be attributed to the presence of compensation effects, which are difficult to avoid.[42−44]

Concluding Remarks

The experimental investigation of silica acid surfaces, by using PEA as a basic probe, has been pursued. The kinetic interpretation of the PEA desorption profiles collected at various heating rates by a computational model that takes into account simultaneous desorption reactions furnished the distribution of the surface acid sites, taking into account their number and energy in a more appropriate way than those of the conventional models. Even in the case of poorly resolved desorption profiles without clearly detectable T_{max} values, it was possible to obtain a reliable kinetic interpretation of the acid-site distribution.

The number of strong acid sites on the modified oxide surface can be expressed in relation to the number of Al, Ti, or Zr surface species that were introduced into the modified silica surfaces. The acid distribution of the studied surfaces is represented by different site types of various acid strength that depend on the nature of the guest element introduced into the silica structure. The possibility of governing the acidity of oxide materials by chemical modification and determining combinations with well-defined acid properties is of great importance from a practical and theoretical point of view. Several models depicting different mechanisms for the acidity generation in mixed-oxide formulations are well known. The central idea of Tanabe[46] is that the acidity is generated by excess negative or positive charge (unbalanced charge density) in the model structure of the modified oxide. Tanaka and Ozaki[47] explain the acidity of modified oxides as being related to the average electronegativities of the metallic ions, and Gervasini et al.[6] rationalized a defined acidity/basicity scale of modified oxide surfaces according to the ion-specific effect (ISE). However, the validity of the hypotheses for acidity prediction is questionable because of the important parameters affecting the acidity of the surface site (nature, concentration, electronic and geometric environment, distance among sites, preparation modality, etc.). A representative case is silica−titania, which has been considered to be a strongly acidic material,[48] also exceeding the acidity of silica−alumina. Its acid properties are strongly related to TiO_2 concentration.[48] Silica−titanias containing low TiO_2 concentration show very low acid character, as found in the present study that confirms our previous findings.[49]

Acknowledgment. We thank Dr. I. Campostrini (Dipartimento di Scienze della Terra Ardito Desio, Università di Milano, Italy) for performing SEM-EDS measurements. Miss C. Della Pina and Miss M. Lazzarin are gratefully acknowledged for their experimental support.

References and Notes

(1) Kung, M. C.; Kung, H. H. *Catal. Rev.—Sci. Eng.* **1985**, *27*, 425.
(2) Auroux, A.; Gervasini, A.; Guimon, C. *J. Phys. Chem. B* **1999**, *103*, 7195.
(3) Borade, R.; Sayari, A.; Adnot, A.; Kaliaguine, S. *J. Phys. Chem.* **1990**, *94*, 5989.
(4) Haw, J. F.; Chuang, I. S.; Hawkins, B. L.; Maciel, G. E. *J. Am. Chem. Soc.* **1983**, *105*, 7206.
(5) Gervasini, A.; Auroux, A. *J. Phys. Chem.* **1990**, *94*, 6372.
(6) Gervasini, A.; Bellussi, G.; Fenyvesi, J.; Auroux, A. *J. Phys. Chem.* **1995**, *99*, 5117.
(7) Gervasini, A.; Fenyvesi, J.; Auroux, A. *Langmuir* **1996**, *12*, 5356.
(8) Mueller, R.; Kammler, H. K.; Wegner, K.; Pratsinis, S. E. *Langmuir* **2003**, *19*, 160.
(9) Gorte, R. J. *Catal. Today* **1988**, *42*, 239.
(10) Karge, H. G.; Dondur, V. *J. Phys. Chem.* **1990**, *94*, 765.
(11) Karge, H. G.; Dondur, V.; Weitkamp, J. *J. Phys. Chem.* **1991**, *95*, 283.
(12) Kreuzer, H. J. *Langmuir* **1992**, *8*, 774.
(13) Abello, M. C.; Velasco, A. P.; Gomez, M. F.; Rivarola, J. B. *Langmuir* **1997**, *13*, 2596.
(14) Payne, S. H.; Kreuzer, H. J. *Surf. Sci.* **1998**, *399*, 135.
(15) Müller, T.; Flynn, G. W. *Langmuir* **2003**, *19*, 2812.
(16) Forni, L.; Magni, E.; Ortoleva, E.; Monaci, R.; Solinas, V. *J. Catal.* **1988**, *112*, 444.
(17) Arena, F.; Dario, R.; Parmaliana, A. *Appl. Catal., A* **1998**, *170*, 127.
(18) Rudzinski, W.; Borowiecki, T.; Panczyk, T.; Dominko, A. *Langmuir* **2000**, *16*, 8037.
(19) Gargiulo, M. V.; Sales, J. L.; Ciacera, M.; Zgrablich, G. *Surf. Sci.* **2002**, *501*, 282.
(20) Kanervo, J. M.; Reinikaiiinen, K. M.; Krause, A. O. I. *Appl. Catal., A* **2004**, *258*, 135.
(21) Cvetanovic, R. J.; Amenomiya, Y. *Catal. Rev.* **1972**, *16*, 21.
(22) Petrovic, Z.; Zavargo, Z. Z. *J. Appl. Polym. Sci.* **1986**, *32*, 4353.
(23) Rakic, V.; Dondur, V.; Misljenovic, D. *J. Therm. Anal.* **1992**, *38*, 879.
(24) Chan, J. H.; Balke, S. T. *Polym. Degrad. Stab.* **1997**, *57*, 135.
(25) Carniti, P.; Gervasini, A.; Auroux, A. *J. Catal.* **1994**, *150*, 274.
(26) Carniti, P.; Gervasini, A.; Ragaini, V. *J. Chem. Soc., Faraday Trans.* **1997**, *93*, 1641.
(27) Gervasini, A.; Carniti, P.; Auroux, A. *Thermochim. Acta* **2001**, *379*, 95.
(28) Carniti, P.; Gervasini, A.; Auroux, A. *Langmuir* **2001**, *17*, 6938.
(29) Cano-Serrano, E.; Blanco-Brieva, G.; Campos-Martin, J. M.; Fierro, J. L. G. *Langmuir* **2003**, *19*, 7621.
(30) Corma, A. *Chem. Rev.* **1995**, *95*, 559.
(31) Bennici, S.; Gervasini, A.; Ravasio, N.; Zaccheria, F. *J. Phys. Chem. B* **2003**, *107*, 5168.
(32) Tanaka, H. *Thermochim. Acta* **1995**, *267*, 29.
(33) Eigenmann, F.; Maciejewski, M.; Baiker, A. *Thermochim. Acta* **2000**, *359*, 131.

(34) Chevrot, V.; Llewellyn, P. L.; Rouquerol, F.; Godlewski, J.; Rouquerol, J. *Thermochim. Acta* **2000**, *369*, 77.
(35) Rouquerol, J. *Therm. Anal. Cal*. **2003**, *72*, 1081.
(36) Carniti, P.; Gervasini, A. Presented at the 5th European Congress on Catalysis, EUROPACAT-V, Limerick, Ireland, Sept 2−7, 2001.
(37) Perego, C.; Amarilli, S.; Carati, A.; Flego, C.; Pazzucconi, G.; Rizzo, C.; Bellussi, G. *Microporous Mesoporous Mater*. **1999**, *27*, 345.
(38) Serrano, D. P.; Uguina, M. A.; Ovejero, G.; Van Grieken, R.; Camacho, M. *Microporous Mesoporous Mater.* **1995**, *4*, 273.
(39) Kissinger, H. E. *Anal. Chem*. **1957**, *29*, 1702.
(40) Buzzi-Ferraris, G. *Ing. Chim. Ital.* **1968**, *4*, 171, 180.
(41) Carnahan, B.; Luther, H. A.; Wilkes, J. O. *Applied Numerical Methods*; Wiley: New York, 1969; p 361.
(42) Bligaard, T.; Honkala, K.; Logadottir, A.; Nørskov, J. K.; Dahl, S.; Jacobsen, C. J. *J. Phys. Chem. B* **2003**, *107*, 9325.
(43) Patterson, W. R.; Rooney, J. J. *J. Catal.* **1994**, *146*, 310.
(44) Rooney, J. J. *Catal. Lett.* **1998**, *50*, 15.
(45) Gellman, A. J.; Paserba, K. R. *J. Phys. Chem. B* **2002**, *106*, 13 231.
(46) Tanabe, K. In *Solid Acid and Base Catalysts*; Catalysis Science and Technology; Anderson, J. R., Boudart, M., Eds.; Springer: Berlin, 1981; Vol. 2, Chapter 5, p 231.
(47) Tanaka, K. I.; Ozaki, A. *J. Catal.* **1967**, *8*, 1.
(48) Itoh, M.; Hattori, H.; Tanabe, K. *J. Catal.* **1974**, *35*, 225.
(49) Carniti, P.; Gervasini, A.; Bernardelli, S. *Polym. Degrad. Stab.* **1997**, *57*, 301.